catalysts

MDPI

Article

The Preparation of a Highly Efficient $Ag_3PO_4/Ag/Bi_2O_2CO_3$ Photo-Catalyst and the Study of Its Photo-Catalytic Organic Synthesis Reaction Driven by Visible Light

Zhi Guo, Hui Xin, Jingjing Ma, Meifen Bai, Yan Wang and Jingyi Li *

College of Chemistry and Chemical Engineering, Inner Mongolia University, Hohhot 010021, China; 761737704@qq.com (Z.G.); 171724951@qq.com (H.X.); ziluobo2010@qq.com (J.M.); 1105187121@qq.com (M.B.); 654164408@qq.com (Y.W.)

* Correspondence: lijingyicn@163.com; Tel.: +86-138-4812-9221

Received: 18 August 2017; Accepted: 14 September 2017; Published: 17 September 2017

Abstract: $Ag_3PO_4/Ag/Bi_2O_2CO_3$ composites were prepared by a hydrothermal and precipitation method. The morphology, structure, and valence state of the photo-catalysts were characterized by X-ray diffraction (XRD), X-ray photoelectron spectroscopy (XPS), transmission electron microscopy (TEM), Scanning electron microscopy (SEM), Brunauer-Emmett-Teller (BET) specific surface areas, and UV-vis diffuse reflectance spectra (UV-vis DRS). They were applied as heterogeneous catalysts in the synthesis of esters from aldehydes (or alcohols) and alcohols and the synthesis of imines from alcohols and amines under visible light irradiation. The photo-catalytic activities of the esterification reactions of aldehydes and alcohols were heavily dependent on the loading of $Ag_3PO_4/Ag/Bi_2O_2CO_3$ as well as the intensity and wavelength of the visible light. Furthermore, their conversion under visible light irradiation was superior to that in the dark. Herein a reaction mechanism from aldehydes and alcohols to esters was proposed, and the $Ag_3PO_4/Ag/Bi_2O_2CO_3$ catalysts could be used six times without a significant decrease in activity. Using these catalysts under visible light could motivate future studies to develop efficient recyclable photo-catalysts and facilitate many synthetic organic reactions.

Keywords: $Ag_3PO_4/Ag/Bi_2O_2CO_3$ photo-catalysts; esterification; amination; visible light

1. Introduction

As two of the most important functional groups in organic chemistry, ester and amine groups have been widely used in the synthesis of fine chemicals, pharmaceutical intermediates, and polymers [1,2]. In recent years, the question of how to produce esters and amines rapidly, effectively and in an energy-efficient manner has attracted great attention [3]. Traditionally, esters have been produced through the reaction of acid derivatives (such as acid chlorides or anhydrides) and alcohols, while imines have been created through the condensation of aldehydes or ketones and amines. However, myriads of by-products are generated as part of these synthetic processes, which both wastes resources and creates environmental pollution [4–6]. Recently, precious metal catalysts supported on carriers (such as Ir [7,8], Cu [9,10], Pd [11], and Au [12]) have been applied in the above-mentioned synthetic processes. However, the reaction conditions have been severe, for example, equivalents of metal salts or metal oxides (such as $KMnO_4$ [13], MnO_2 [14] or $KHSO_4$ [15]) were added as oxidants, which created many by-products in the reaction, thus making the utilization ratio of the raw material unfavorable [16–20]. Therefore, it is important to discover an alternative to produce esters from aldehydes (or alcohols) and alcohols, and imines from alcohols and amines by using solid catalysts for the purposes of green chemistry and organic synthesis under milder conditions.

Photo-catalysis is of interest in green chemistry as it can improve catalytic efficiency and use visible light. Photo-catalysis has been regarded as one of the most effective ways to address energy shortages and environmental pollutions [21,22]. Many researchers have expressed an interest in Bi materials due to their special semiconductor layered crystal structures and d^{10} electron configurations, which enable them to respond to light [23–25]. Consisting of $(Bi_2O_2)^{2+}$ and $(CO_3)^{2-}$ layers, $Bi_2O_2CO_3$ [26–29], a member of the stratified or Aurivillius-related oxide family, has demonstrated good performance in antibacterial [28,29] and environmental applications [26,30–33]. However, it has a poor ability to separate electrons and holes which was poor after excitation by visible light, therefore, many efforts have been made to decrease its recombination of electrons and holes in order to enhance its photo-catalytic activity. These efforts have included the construction of two-dimensional (2D) or three-dimensional (3D) structures [26,30–33], and the interaction of $Bi_2O_2CO_3$ with $BiVO_4$ [34], graphene [35], Fe_3O_4 [36], and BiOCl [37] among others. Recently, Ag-based compounds (such as Ag_3PO_4 [38] and Ag@AgX (X = Cl, Br, I)) [39–41] have been widely studied as theoretically promising photo-catalytic materials [42], where the filled d^{10} electronic configuration unique to Ag^+ could take part in the formation and hybridization of the energy band structure (such as Ag-based composites) [43–45]. The semiconductor Ag_3PO_4, with a band gap of 2.45 eV, could be activated by visible light, retrieve O_2 from water, and degrade organic dyes [46]. Furthermore, its solid-state structure could improve the transfer capability of the photo-generated electrons through interactions between the metal and semiconductor materials. Therefore, optimizing the interaction between the metals and semiconductors is of great importance [22].

In the composites, Ag_3PO_4 and $Bi_2O_2CO_3$ the composites were excited by visible light, and electrons and holes were transferred by Ag. Under visible light irradiation, electrons and holes were generated by Ag_3PO_4, the Fermi level of Ag was more positive than the conduction band of Ag_3PO_4, so electrons on the conduction band of Ag_3PO_4 could transfer to Ag. Similarly, under visible light irradiation, electrons and holes were also generated by $Bi_2O_2CO_3$, but the Fermi level of Ag was more negative than the valence band of $Bi_2O_2CO_3$, so the holes were easily transferred to Ag. Ag can act as a trap for electrons as usually happens in semiconductor/metal nanoparticle systems. Therefore, the composite material had a strong redox ability [34,37,47]. Through the analysis of each component of the composite material, it was found that a variety of organic reactions could be carried out under visible light irradiation. The esterification of aldehydes (or alcohols) and alcohols, and the amination of alcohols and amines were detected over $Ag_3PO_4/Ag/Bi_2O_2CO_3$ under visible light irradiation. Additionally, the effects of light intensity and wavelength on the esterification procedure of aldehydes and alcohols were examined. The conversion sped up when the light intensity increased, confirming that the reaction was initiated by visible light, thus, light between 400 and 650 nm played an important role. Furthermore, this catalyst continued to manifest high activity after being used six times. Finally, a possible mechanism from aldehydes and alcohols to esters was proposed, based on the experimental evidence and correlated documents.

2. Results and Discussion

2.1. Phase Stucture (XRD)

The phase structures of different metals or metal composites were detected by X-ray diffraction (XRD) (Rigaku Industrial Corporation, Osaka, Japan) (Figure 1). Sharp and intense diffraction peaks of the prepared $Bi_2O_2CO_3$ appeared, which were ascribed to a tetragonal phase of $Bi_2O_2CO_3$ (JCPDS Card No. 41-1488, a = 3.865 Å, b = 3.865 Å, and c = 3.675 Å). Four apparent diffraction peaks were observed at 23.90°, 30.25°, 32.73°, and 46.97°, which could be assigned as the (011), (013), (110), and (020) lattice planes of tetragonal $Bi_2O_2CO_3$, respectively. In addition, XRD peaks at 23.90°, 30.25°, 32.73°, and 46.97° were observed for the composite of Ag on the $Bi_2O_2CO_3$ surface. However, no Ag peaks were observed, which may have been a consequence of overly small Ag particles [48]. The diffraction peaks of the Ag_3PO_4 composite on the $Bi_2O_2CO_3$ surface were the same as those of cubic Ag_3PO_4 (JCPDS

Card No. 06-0505), demonstrating that Ag_3PO_4 was successfully deposited onto the $Bi_2O_2CO_3$ surface. The cubic Ag_3PO_4 diffraction peaks were clearly observed in the $Ag_3PO_4/Ag/Bi_2O_2CO_3$ catalyst diffraction pattern, while the diffraction peaks associated with the $Bi_2O_2CO_3$ component disappeared. This phenomenon may have been caused by the coverage of Ag_3PO_4 after depositing Ag_3PO_4 and Ag on $Bi_2O_2CO_3$ [22]. The diffraction peaks of $Bi_2O_2CO_3$ at 30.25° and 32.73° coincide with that of Ag_3PO_4 at 29.70° and 33.29° in the $Ag_3PO_4/Ag/Bi_2O_2CO_3$ catalyst diffraction pattern (Figure 1a).

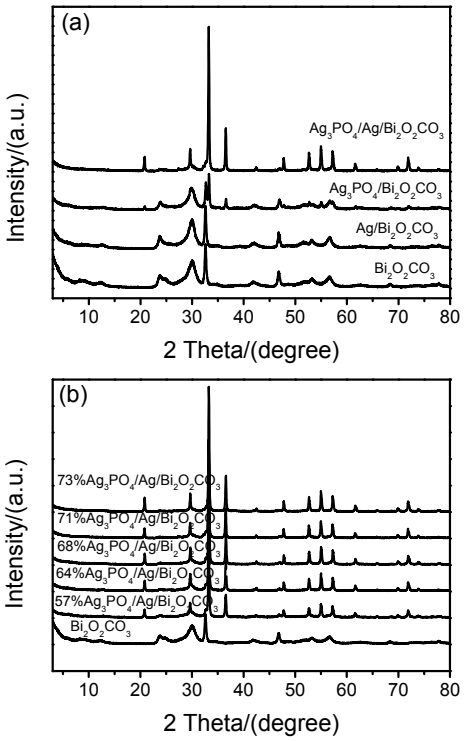

Figure 1. X-ray diffraction (XRD) patterns of the different photo-catalysts. (**a**) XRD of the different catalysts (**b**) XRD of the different amounts of $Ag_3PO_4/Ag/Bi_2O_2CO_3$ catalysts.

The phase structures of the catalysts prepared with different silver phosphate loadings were also investigated by XRD (Figure 1b). The cubic Ag_3PO_4 diffraction peaks were clearly detected, and the intensity of these peaks gradually increased with increasing Ag_3PO_4 ratio in the composite.

2.2. Chemical Composition (XPS)

X-ray photoelectron spectroscopy (XPS) was performed to assay the chemical composition and chemical state of the Ag element in the $Ag_3PO_4/Ag/Bi_2O_2CO_3$ composites. The Bi 4f XPS spectra are elaborated in Figure 2a, where two peaks at 159.58 and 164.78 eV were observed. Thus, the dominant chemical state of Bi in the $Ag_3PO_4/Ag/Bi_2O_2CO_3$ catalyst can be regarded as +3 [49]. The peaks at 368.34 and 374.50 eV were caused by Ag $3d_{5/2}$ and Ag $3d_{3/2}$, respectively (Figure 2b). The Ag $3d_{5/2}$ peaks were further separated into two peaks at 368.2 and 368.55 eV, and the Ag $3d_{3/2}$ peak was also separated into two peaks at 374.2 and 374.5 eV. The peaks at 368.2 and 374.2 eV were caused by the Ag^+ of Ag_3PO_4, and the peaks at 368.55 and 374.5 eV corresponded to Ag^0 [50,51]. In Figure 2c, a single O 1s peak at 531.38 eV was observed, and attributed to the carbonate species [52]. A broad P 2p peak within the range of 131.38 to 136.18 eV (Figure 2d) was observed for the $Ag_3PO_4/Ag/Bi_2O_2CO_3$ sample, which corresponded to the phosphorus (P) of Ag_3PO_4 [53]. The presence of Ag and Ag_3PO_4 in the prepared composites was confirmed by XPS analysis.

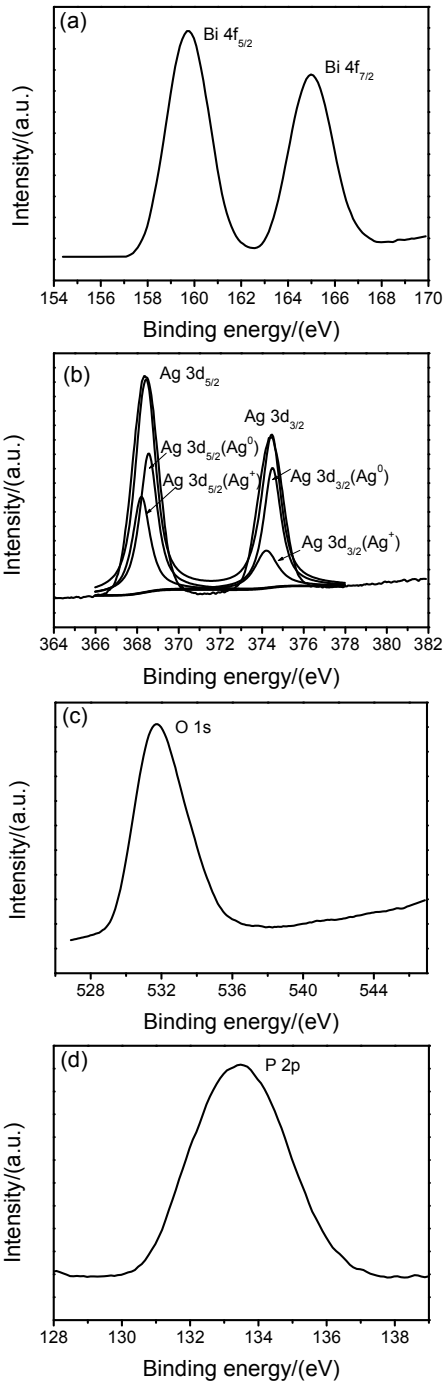

Figure 2. X-ray photoelectron spectroscopy (XPS) spectra of Bi 4f, Ag 3d, O 1s, and P 2p of the 71 wt % $Ag_3PO_4/Ag/Bi_2O_2CO_3$ composite. (**a**) XPS of Bi (**b**) XPS of Ag (**c**) XPS of O (**d**) XPS of P.

2.3. Morphological Structure (TEM, Energy Dispersive X-ray Spectrum (EDX), and SEM)

The morphology, crystal form, and composition of the composites were elucidated by transmission electron microscopy (TEM), energy dispersive X-ray spectrum (EDX) (Figure 3a–3k), and Scanning electron microscopy (SEM) (Figure S1a–S1j), respectively. The lattice fringes of d = 0.274 and 0.297 nm were attributed to the (110) and (013) planes of the $Bi_2O_2CO_3$ nano-sheets (Figure 3b). This phenomenon was consistent with the XRD results, confirming a successful $Bi_2O_2CO_3$ synthesis. The lattice fringe of d = 0.237 nm was attributed to the (111) plane of Ag (Figure 3d) and those of d = 0.274 nm (0.269 nm) and 0.301 nm (0.299 nm, 0.297 nm) were attributed to the (210) and (200)

planes of cubic Ag_3PO_4 (Figure 3f,h,j). Therefore, Ag_3PO_4 was successfully loaded onto the $Bi_2O_2CO_3$ material. The EDX image (Figure 3k) of the 71 wt % $Ag_3PO_4/Ag/Bi_2O_2CO_3$ composite demonstrated that Ag_3PO_4, Ag, and $Bi_2O_2CO_3$ particles were all present within the catalyst, which confirmed the successful formation of a three-phase nanoparticle hetero-structure.

Pure $Bi_2O_2CO_3$ is porous and spherical. Its particle size was approximately 117.8 μm (Figure S1a,b). The different photo-catalysts (Figure S1c–h) consisted of spherical particles with average diameters of 112.0, 126.0, and 208.9 μm for the 10 wt % $Ag/Bi_2O_2CO_3$, 64 wt % $Ag_3PO_4/Bi_2O_2CO_3$, and 71 wt % $Ag_3PO_4/Ag/Bi_2O_2CO_3$ composites, respectively. However, the particle shapes became irregular after the materials were used six times (Figure S1i,j). The spherical structures consisted of nano-sheets (Figures S1a–h).

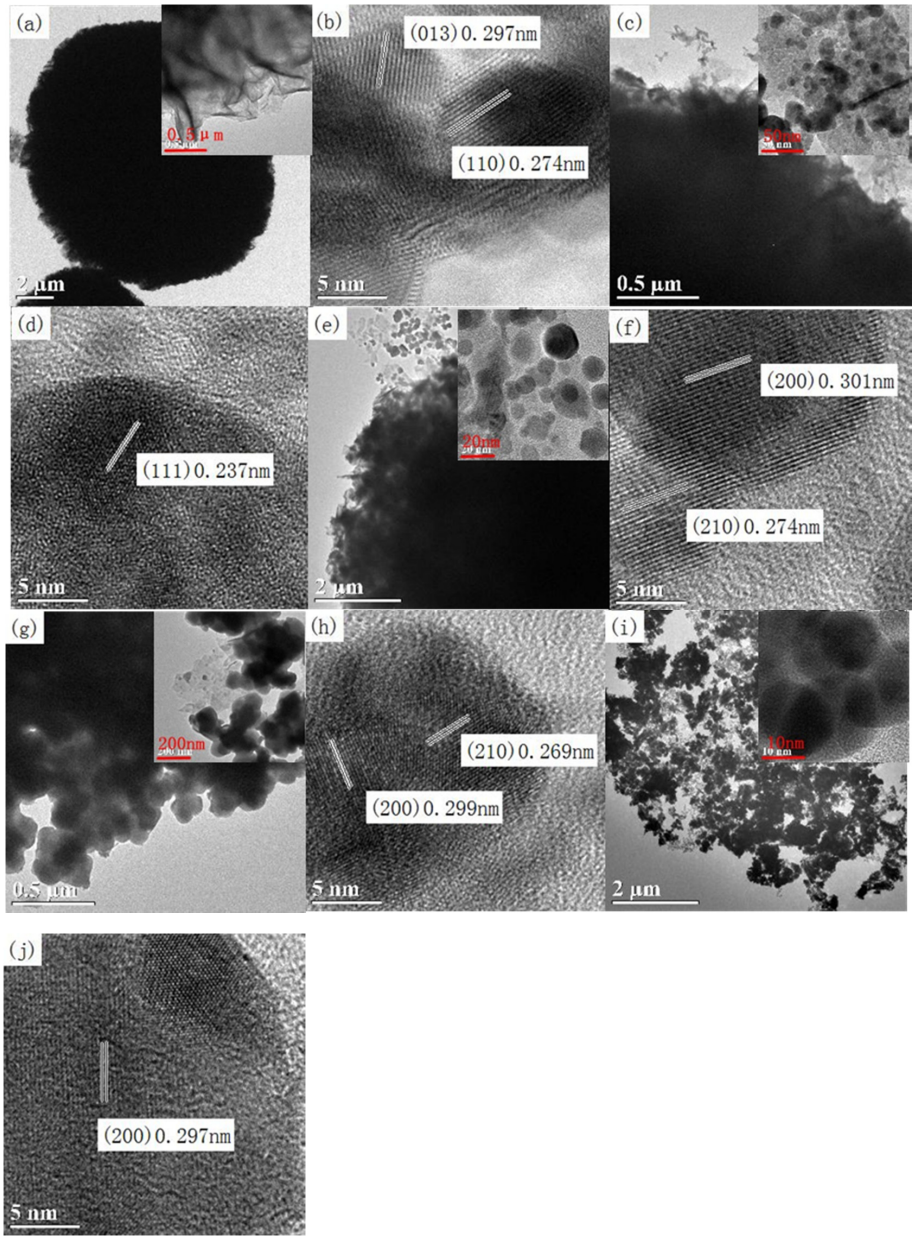

Figure 3. *Cont.*

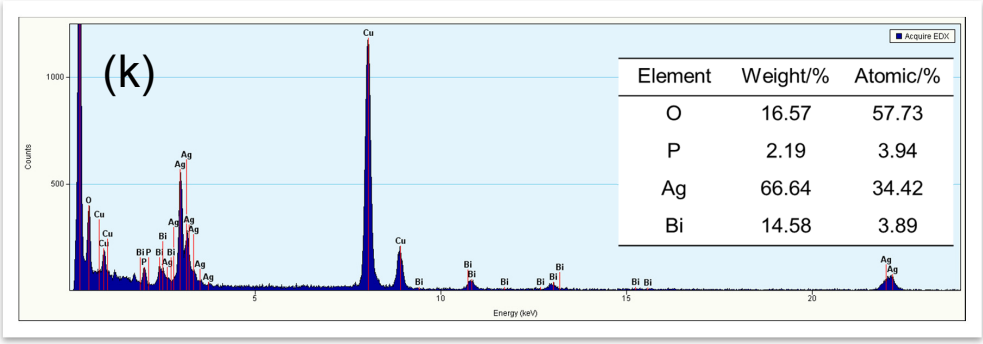

Figure 3. TEM, high resolution transmission electron microscopy (HRTEM), and energy dispersive X-ray spectrum (EDX) patterns of the photo-catalysts (**a**,**b**) $Bi_2O_2CO_3$; (**c**,**d**) 10 wt % $Ag/Bi_2O_2CO_3$; (**e**,**f**) 64 wt % $Ag_3PO_4/Bi_2O_2CO_3$; (**g**,**h**) 71 wt % $Ag_3PO_4/Ag/Bi_2O_2CO_3$; (**i**,**j**) reused 71 wt % $Ag_3PO_4/Ag/Bi_2O_2CO_3$; and (**k**) EDX image of 71 wt % $Ag_3PO_4/Ag/Bi_2O_2CO_3$.

2.4. Specific BET Surface Areas

The BET surface areas of these catalysts are given in Table S1. The surface area of pure $Bi_2O_2CO_3$ was 51.05 $m^2 \cdot g^{-1}$, and it dwindled to 46.11 $m^2 \cdot g^{-1}$ after the Ag loading onto the $Bi_2O_2CO_3$ surface. The decrease in the surface area of $Ag/Bi_2O_2CO_3$ predominantly resulted from the Ag loading onto the $Bi_2O_2CO_3$ surface. With the increase in Ag_3PO_4 mass ratio, the corresponding surface area decreased dramatically (Table S1), possibly as a result of filling Ag_3PO_4 gradually into the mesoporous structure of $Bi_2O_2CO_3$.

2.5. UV-Vis DRS and Band Gap

UV-vis diffuse reflectance spectra (DRS) were used to calculate the band gap and light absorbing ability of the photo-catalysts. An absorption peak appeared within the UV range for all samples (Figure 4). For 10 wt % $Ag/Bi_2O_2CO_3$, the absorption within the 400–800 nm range was attributed to the surface plasmon resonance (SPR) of the Ag nanoparticles. The absorption of 64 wt % $Ag_3PO_4/Bi_2O_2CO_3$ was greater than that of $Bi_2O_2CO_3$ within the 400–800 nm range due to the presence of Ag_3PO_4. In addition, a stronger absorption within the 400–800 nm range occurred for the 10 wt % $Ag/Bi_2O_2CO_3$ and 64 wt % $Ag_3PO_4/Bi_2O_2CO_3$ composites. Furthermore, a much stronger absorption was present within the 400–800 nm range for the 71 wt % $Ag_3PO_4/Ag/Bi_2O_2CO_3$ composite compared to 64 wt % $Ag_3PO_4/Bi_2O_2CO_3$. Overall, a strong absorption capacity of the 71 wt % $Ag_3PO_4/Ag/Bi_2O_2CO_3$ composite was detected within the visible light range (Figure 4a).

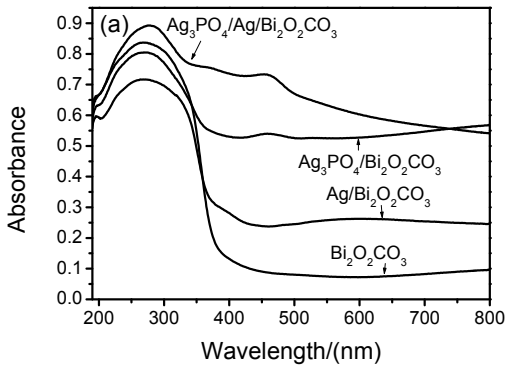

Figure 4. *Cont.*

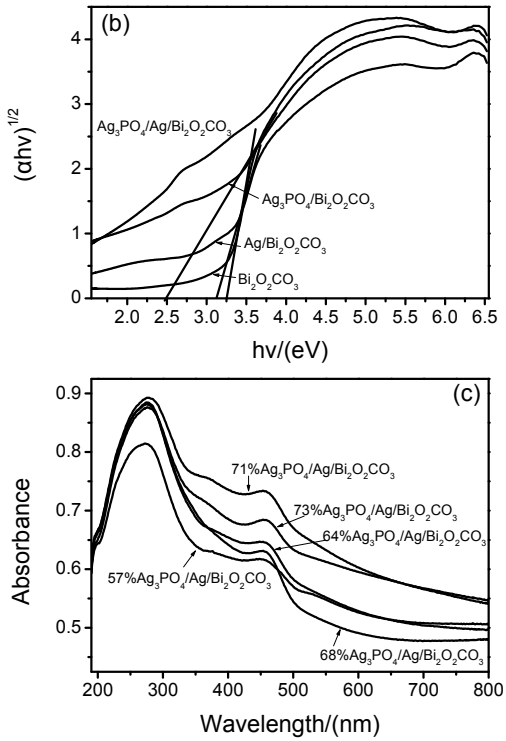

Figure 4. UV-vis diffuse reflectance spectra of the different photo-catalysts. (**a**) UV-vis DRS of the different catalysts (**b**) UV-vis DRS transferring spectra-$(\alpha h\nu)^{1/2}$~$h\nu$ of the different catalysts (**c**) UV-vis DRS of the different amounts of $Ag_3PO_4/Ag/Bi_2O_2CO_3$ catalysts.

The optical absorption near the band edge was in agreement with Equation (1) for a crystalline semiconductor [54].

$$\alpha(h\nu) = A(h\nu - E_g)^{n/2} \quad (1)$$

Here, α, ν, A, n, and E_g represented the diffuse absorption coefficient, the light frequency, a proportionality constant, an integer (n = 1, 2, 4, 6), and the band gap energy, respectively. In the case of the $Bi_2O_2CO_3$ material [27], the value of n was 4. As shown in Figure 4b, the estimated E_g was 3.25 eV for $Bi_2O_2CO_3$, which was consistent with the literature value [32,35]. The absorption peak of the 64 wt % $Ag_3PO_4/Bi_2O_2CO_3$ composite within the 400–800 nm range was attributed to Ag_3PO_4, while the absorption peak between 200 and 400 nm was ascribed to $Bi_2O_2CO_3$ and Ag_3PO_4. The absorption peak of cubic Ag_3PO_4 within the 400–800 nm range was observed (Figure 4c). Further analysis demonstrated that the absorption peak of the 73 wt % $Ag_3PO_4/Ag/Bi_2O_2CO_3$ catalyst was weaker than that of the 71 wt % $Ag_3PO_4/Ag/Bi_2O_2CO_3$ catalyst. Therefore, the strongest light absorption corresponded to the 71 wt % $Ag_3PO_4/Ag/Bi_2O_2CO_3$ composite, which further explained why the catalytic activity of this material was better than that of the 73 wt % $Ag_3PO_4/Ag/Bi_2O_2CO_3$ composite.

2.6. Photo-Catalytic Activities

2.6.1. Esterification of Aldehydes and Alcohols

The photo-catalytic performance of the $Ag_3PO_4/Ag/Bi_2O_2CO_3$ composites was investigated by the photo-catalytic oxidative esterification of benzaldehyde (1.5 mmol) and methanol (8 mL) under certain initial conditions under visible light (including 64 wt % $Ag_3PO_4/Ag/Bi_2O_2CO_3$ (50 mg), temperature of 35 ± 3 °C, and an Ar atmosphere). The products were detected by gas chromatography (GC). A benzaldehyde conversion of 80.6% was achieved after 48 h with a corresponding selectivity of 99.5% for methyl benzoate. The reaction conditions were optimized by choosing 8 mL of methanol as a

solvent, 1.0 mmol of benzaldehyde as a reactant, and 30 mg of catalyst under advantageous conditions such as 35 ± 3 °C, an Ar atmosphere, and normal atmospheric pressure.

The reactions of benzaldehyde with different alcohols were investigated by using 71 wt % $Ag_3PO_4/Ag/Bi_2O_2CO_3$. Methanol provided the desired products at a higher conversion (Table 1, entries 1–6). The corresponding benzoate esters were produced by ethanol, isopropanol, butanol, octanol, and 2-octanol under visible light irradiation. The nucleophilicity between the secondary alcohol and the long chain carbon alcohol was weak; however, aldehyde conversions were below 10% in all cases when the reactions were performed in the dark (Table 1). Different substituted benzaldehydes were transformed to the corresponding esters under the same conditions (Table 1, entries 7–12). Aldehyde conversions of 95.5% and 99.4% were reached (Table 1, entries 7 and 8). The substituted benzaldehyde conversions with an electron-withdrawing group reached only 66.2% and 48.6% (Table 1, entries 9 and 10). In contrast, the substituted benzaldehydes with electron-donating groups proved more advantageous for the esterification reaction than those with electron-withdrawing groups. The more stable the radical resonance structure, the higher was the reactant conversion. In contrast, when electron-withdrawing groups were located at the counter point of the benzene ring, free radical resonance structures were formed that were unstable and disadvantageous for the esterification reaction. Even reactive hetero-cycles with a long-chain aliphatic aldehyde, such as furfuraldehyde or valeraldehyde, could be transformed into the corresponding esters with modest conversions (52.6% and 40.1%, Table 1, entries 11 and 12). Both electron-withdrawing and electron-donating benzylic aldehydes worked for this transformation using silver photo-catalysts.

Table 1. Synthesis of esters from different aldehydes and alcohols using 71 wt % $Ag_3PO_4/Ag/Bi_2O_2CO_3$.

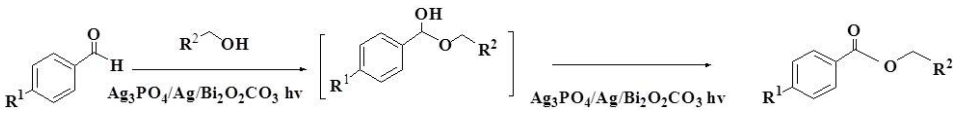

Entry	Aldehyde	Alcohol	In the Visible Light		In the Dark	
			Conversion (%)	Selectivity (%)	Conversion (%)	Selectivity (%)
1		Methanol	88.3	>99	8.2	>99
2		Ethanol	86.9	>99	3.5	>99
3		Isopropanol	61.7	>99	1.6	>99
4		Butanol	86.3	>99	0.1	>99
5		Octanol	37.0	84.3	3.5	40.2
6		2-Octanol	15.9	50.3	5.2	30.1
7	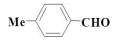	Methanol	95.5	>99	0.6	>99
8	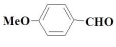	Methanol	99.4	>99	0.7	>99
9	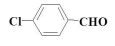	Methanol	66.2	>99	0.7	>99
10	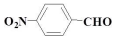	Methanol	48.6	>99	1.2	>99
11		Methanol	52.6	>99	0.4	>99
12		Methanol	40.1	>99	1.3	>99

Reaction conditions: aldehyde (1.0 mmol) and $Ag_3PO_4/Ag/Bi_2O_2CO_3$ catalyst (30 mg) were added to alcohol (8 mL). The reaction flask was stirred magnetically and was irradiated with a 500 W Philips halogen lamp (wavelength range of 400–800 nm, and a light intensity of 2.5×10^{-2} W·cm^{-2}) as the visible light source under an Ar atmosphere at 35 ± 3 °C. After running for 24 h, the reaction conversion and selectivity were determined by GC.

Subsequently, the effects of the different photo-catalysts and the $Ag_3PO_4/Ag/Bi_2O_2CO_3$ with different Ag_3PO_4 mass ratios were tested (Table 2). After 24 h of visible light irradiation, low

conversions were detected with the $Bi_2O_2CO_3$ support compared with the other metal or metal oxide-loaded photo-catalysts (Table 2, entries 1–3). This observation confirmed that the metal or metal oxide nanoparticles were crucial for the esterification reaction. The photocatalytic esterification of benzaldehyde and methanol was carried out using the $Ag_3PO_4/Ag/Bi_2O_2CO_3$ composites with varied silver phosphate contents (Table 2, entries 4–8). The conversion increased and then decreased with the increasing silver phosphate content. The highest conversion (88.3%) for the esterification of benzaldehyde and methanol was obtained using the 71 wt % $Ag_3PO_4/Ag/Bi_2O_2CO_3$ composite (Table 2, entry 7). Moreover, the conversion conducted in the dark was significantly lower than that under visible light irradiation. Therefore, light was crucial for the reaction process (Table 2, entries 1–8).

Table 2. Synthesis of esters from benzaldehyde and methanol using different photo-catalysts.

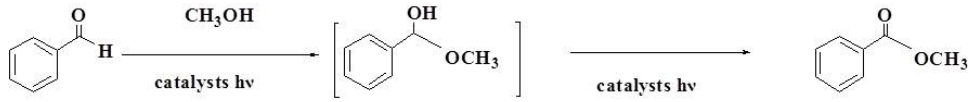

Entry	Catalysts	In the Visible Light		In the Dark	
		Conversion (%)	Selectivity (%)	Conversion (%)	Selectivity (%)
1	$Bi_2O_2CO_3$	33.3	>99	13.1	>99
2	$10\%Ag/Bi_2O_2CO_3$	60.8	>99	12.2	>99
3	$64\%Ag_3PO_4/Bi_2O_2CO_3$	67.8	>99	4.4	>99
4	$57\%Ag_3PO_4/Ag/Bi_2O_2CO_3$	25.7	>99	4.7	>99
5	$64\%Ag_3PO_4/Ag/Bi_2O_2CO_3$	73.0	>99	6.4	>99
6	$68\%Ag_3PO_4/Ag/Bi_2O_2CO_3$	76.0	>99	13.1	>99
7	$71\%Ag_3PO_4/Ag/Bi_2O_2CO_3$	88.3	>99	8.2	>99
8	$73\%Ag_3PO_4/Ag/Bi_2O_2CO_3$	74.8	>99	4.4	>99

Reaction conditions: aldehyde (1.0 mmol) and catalyst (30 mg) were added to alcohol (8 mL). The reaction flask was stirred magnetically and was irradiated with a 500 W Philips halogen lamp (wavelength range of 400–800 nm, and a light intensity of 2.5 × 10−2 W·cm^{-2}) as the visible light source under an Ar atmosphere at 35 ± 3 °C. After running for 24 h, the reaction conversion and selectivity were determined by GC.

2.6.2. Esterification of Alcohols and Alcohols

The catalytic activities of different proportions of Ag_3PO_4 in $Ag_3PO_4/Ag/Bi_2O_2CO_3$ were tested in the esterification reaction of benzaldehyde and methanol where the 71 wt % $Ag_3PO_4/Ag/Bi_2O_2CO_3$ had an excellent catalytic outcome. Therefore, the esterification reactions of alcohols and alcohols were conducted using 71 wt % $Ag_3PO_4/Ag/Bi_2O_2CO_3$ as a catalyst. Benzyl alcohol (1.0 mmol) and methanol (8 mL) were applied in this reaction, which was tested with various bases, different dosages of the base, and different alcohol substitutes and the bases showed a great influence on the reaction. The conversion was highest using Cs_2CO_3 as a base (Table S2, entries 1–5). Finally, the optimized amount of base was 0.6 mmol (Table S2, entries 1, 6–8).

Under the optimized reaction conditions, various fatty alcohols and benzyl alcohol derivatives were rapidly converted to the corresponding esters (Table 3).

Reaction conditions: derivative of benzyl alcohol (1.0 mmol), base (0.6 mmol Cs_2CO_3), and $Ag_3PO_4/Ag/Bi_2O_2CO_3$ catalyst (30 mg) were added to the fatty alcohol derivatives (8 mL). The reaction flask was stirred magnetically and was irradiated with a 500 W Philips halogen lamp (wavelength range of 400–800 nm, and a light intensity of 2.5 × 10^{-2} W·cm^{-2}) as the visible light source under an air atmosphere at 35 ± 3 °C. After running for 24 h, the reaction conversion and selectivity were determined by GC.

Table 3. Synthesis of esters from different alcohols using 71 wt % $Ag_3PO_4/Ag/Bi_2O_2CO_3$.

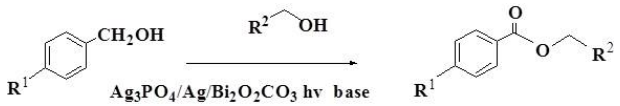

Entry	Alcohol	Alcohol	In the Visible Light		In the Dark	
			Conversion (%)	Selectivity (%)	Conversion (%)	Selectivity (%)
1		Methanol	93.5	75.6	11.1	51.3
2		Ethanol	83.4	73.2	6.8	48.0
3		Isopropanol	8.1	21.5	3.4	0
4		Butanol	71.2	54.0	20.4	21.2
5		Octanol	40.0	61.8	0.1	0
6	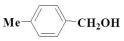	Methanol	72.6	81.8	23.3	>99
7	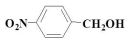	Methanol	37.2	78.6	12.5	>99
8	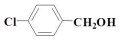	Methanol	55.0	62.7	16.0	>99
9		Methanol	52.5	>99	20.1	>99
10		Methanol	40.1	>99	11.4	>99
11		Methanol	13.6	>99	1.4	>99

2.6.3. Amination of Alcohols and Amines

The synthesis of imines by benzyl alcohol and aniline was studied using the 71 wt % $Ag_3PO_4/Ag/Bi_2O_2CO_3$ catalysts. The influences of solvents and bases were scrutinized to discover the optimal reaction conditions. The highest activity occurred when using Cs_2CO_3 as a base (Table S3, entries 1–5). With Cs_2CO_3 as the base, notable activity was achieved when benzotrifluoride was used as a solvent. The conversion of aniline did not even reach 40% in other solvents (Table S3, entries 6–11). Furthermore, the highest activity occurred when using 0.8 mmol of base (Table S3, entries 1, 12–14).

Different derivatives of alcohols and anilines were examined under the optimized conditions. Good conversions were produced except for *p*-methoxyaniline (Table 4, entries 1–5). In addition, 62.5% and 65.6% conversion were achieved with the allylic alcohols, such as cinnamyl alcohol and crotyl alcohol (Table 4, entries 9 and 11). Meanwhile, furfuryl alcohol was converted by using the catalyst (Table 4, entry 10).

Reaction conditions: alcohol (1.0 mmol), the substitute of aniline (0.5 mmol), base (0.8 mmol Cs_2CO_3), and $Ag_3PO_4/Ag/Bi_2O_2CO_3$ catalyst (30 mg) were added to benzotrifluoride (6 mL). The reaction flask was stirred magnetically and was irradiated with a 500 W Philips halogen lamp (wavelength range of 400–800 nm, and a light intensity of 2.5×10^{-2} W·cm^{-2}) as the visible light source under an air atmosphere at 35 ± 3 °C. After running for 24 h, the reaction conversion and selectivity were determined by GC.

Table 4. Synthesis of imines from benzyl alcohol and aniline substitutes using 71 wt % $Ag_3PO_4/Ag/Bi_2O_2CO_3$.

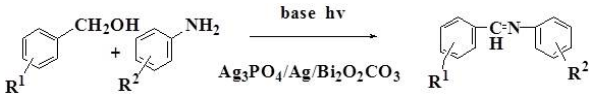

Entry	Alcohol	Amine	In the Visible Light		In the Dark	
			Conversion (%)	Selectivity (%)	Conversion (%)	Selectivity (%)
1			80.5	>99	10.1	>99
2			92.0	>99	6.8	>99
3	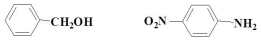		94.0	>99	3.4	>99
4			81.2	>99	10.4	>99
5			55.9	>99	0.1	>99
6	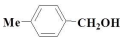		71.8	80.7	13.3	>99
7	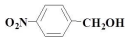		94.0	83.7	12.5	>99
8	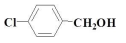		79.1	77.2	11.0	>99
9	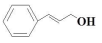		62.5	>99	10.1	>99
10			40.1	>99	11.4	>99
11			65.6	>99	1.4	>99

2.7. Effect of Light Intensity and Wavelength

To certify that the reaction was photo-catalytic and that the light intensity and wavelength had an important influence on the reaction process [55,56], experiments were performed using different light intensities and wavelengths (Figures 5 and 6). The contributions of light irradiation were determined by subtracting the conversion in the dark from the overall conversion under light irradiation, equalizing both reactions at the same reaction temperature. Here, the conversion in the dark was seen as the contribution of the thermal effect. First, the conversion of benzaldehyde increased gradually with the increase in light intensity (Figure 5), whereas the conversion of benzaldehyde changed little in the dark, which indicated that the reaction was activated by light. Typically, when the light intensity was 0.01 $W \cdot cm^{-2}$, the overall conversion was 64.9%, of which the light contribution to the overall process was 87%, while the thermal contribution accounted for only 13% at 35 ± 3 °C. More importantly, when the light intensity was increased from 0.01 $W \cdot cm^{-2}$ to 0.043 $W \cdot cm^{-2}$, the conversion of reactants increased dramatically from 64.9% to 96.8%. This result further demonstrated that the light intensity played a significant role in the reaction process. When the light intensity was stronger, more energy was provided, and more electrons and holes were produced by Ag_3PO_4 and $Bi_2O_2CO_3$. The faster the transfer rate of the electrons and holes, the more prominent was the light contribution to the conversion of benzaldehyde.

The effects of different wavelength ranges on the esterification reaction of aldehydes and alcohols are shown in Figure 6. First, the wider the wavelength range, the higher was the conversion of benzaldehyde. In other words, when the wavelength range was changed from 400–800 nm to 650–800 nm, the conversion of benzaldehyde was reduced. For example, the conversion of benzaldehyde was 85.7%, when the wavelength range was between 400 and 800 nm. However, the conversion was 78.3%, when the wavelength range was monitored between 450 and 800 nm. The conversion was only 20.5%, when the wavelength range was restricted between 650 and 800 nm with equal irradiation intensity. In addition, the reaction conversion was 8.5% in the dark at the same temperature. A minor change occurred with wavelengths longer than 650 nm or shorter than 450 nm; 91% of the total benzaldehyde conversion was obtained by the contribution of visible light

irradiation between 400 and 800 nm, while the thermal contribution accounted for the other 9%. Using the same calculation method, the contribution of light to the conversion could be calculated in any wavelength range. As shown in Figure 6, when the wavelength range was between 400 and 650 nm, the contribution of light was 85%. The light contributions to the conversion of benzaldehyde between the wavelength ranges of 400–450, 450–510, 510–650, and 650–800 nm were 10%, 44%, 31%, and 15%, respectively. These results were similar to that of the absorption of the silver phosphate nanoparticles between 400 and 800 nm [22]. Therefore, these experimental results indicated that the range of irradiation intensity and wavelength played important roles in the catalytic reaction along with the role of visible light irradiation.

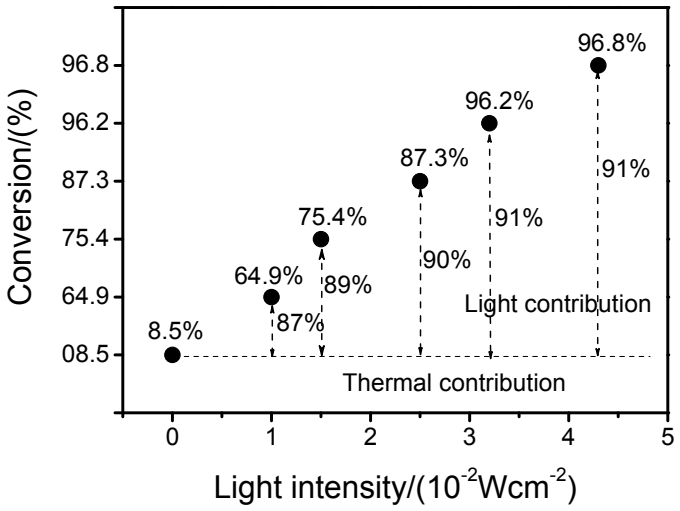

Figure 5. Effect of light intensity on the esterification of benzaldehyde using 71 wt % $Ag_3PO_4/Ag/Bi_2O_2CO_3$.

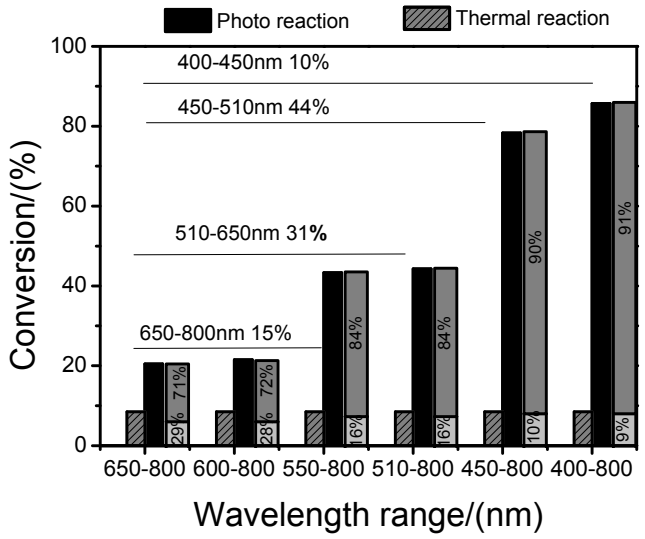

Figure 6. Effect of the light wavelength on the esterification of benzaldehyde using 71 wt % $Ag_3PO_4/Ag/Bi_2O_2CO_3$.

2.8. The Recyclability of the Prepared Catalysts

The conversion using the 71 wt % $Ag_3PO_4/Ag/Bi_2O_2CO_3$ catalyst was the highest for the esterification reaction of aldehydes and alcohols of all the prepared catalysts. To further verify that the catalyst had a stronger application value, a life test of the catalyst was performed and the test results

are shown in Figure S2. The conversion of benzaldehyde and the selectivity of products changed little after it was used four times. Compared to the first four times, the conversion of benzaldehyde dwindled when the catalyst was used for the fifth and sixth times. This could have been due to the loss of some Ag_3PO_4 and Ag nanoparticles during the recycling process, which was in agreement with the TEM (Figure 3i,j) and EDX observations (Figure 3k and Figure S3, and the weight% of Ag changed from 66.64%–18.88% after recycling).

2.9. Reaction Mechanism

Based on the experimental results, a possible mechanism for the photocatalytic esterification of benzaldehyde using $Ag_3PO_4/Ag/Bi_2O_2CO_3$ is presented in Schemes 1 and 2 [22,27]. Ag nanoparticles were located between Ag_3PO_4 and $Bi_2O_2CO_3$. Ag can act as a trap for electrons as usually happens in semiconductor/metal nanoparticle systems. Under visible light irradiation, electrons and holes were produced from $Bi_2O_2CO_3$ and Ag_3PO_4, followed by the transfer of the photo-generated electrons to Ag, while the holes were concentrated on the Ag_3PO_4 due to the close contact between Ag_3PO_4 and $Bi_2O_2CO_3$ (Scheme 1, reactions 1 and 2 and Scheme 2). Therefore, Ag played a major role in the transfer of electrons in the reaction of aldehydes and alcohol. Photo-generated electrons and holes were effectively separated, which granted $Ag_3PO_4/Ag/Bi_2O_2CO_3$ a strong photo-catalytic activity. Therefore, the Ag located between the $Bi_2O_2CO_3$ and Ag_3PO_4 acted as a charge-carrier transfer material during the esterification process of the aldehydes and alcohols, which effectively prolonged the lifetime of the photo-induced holes produced by $Bi_2O_2CO_3$ and Ag_3PO_4. The first step of the reaction involved the loss of a proton from the alcohol to form an alkoxyl radical (Scheme 1, reaction 3 and Scheme 2). Subsequently, the benzaldehyde received an electron and then was reduced to a reactive intermediate, which was then protonized rapidly to generate an α-hydroxyl radical (Scheme 1, reactions 4 and 5 and Scheme 2). Next, the α-hydroxyl radical and alkoxyl radical were combined to generate a relatively stable hemiacetal intermediate (Scheme 1, reaction 6 and Scheme 2). The α-H of the hemiacetal intermediate structure was also attracted by the silver nanoparticles, and hence formed an ester. Finally, H^+ of Ag-H was transferred to the alkoxyl radical to form an alcohol, leaving the silver nanoparticles (Scheme 1, reactions 7-9 and Scheme 2). The silver and silver phosphate nanoparticle surfaces could then be re-activated by visible light, and a new reaction process could begin [57–62] (Scheme 2).

The reactions are shown as follows (Scheme 1):

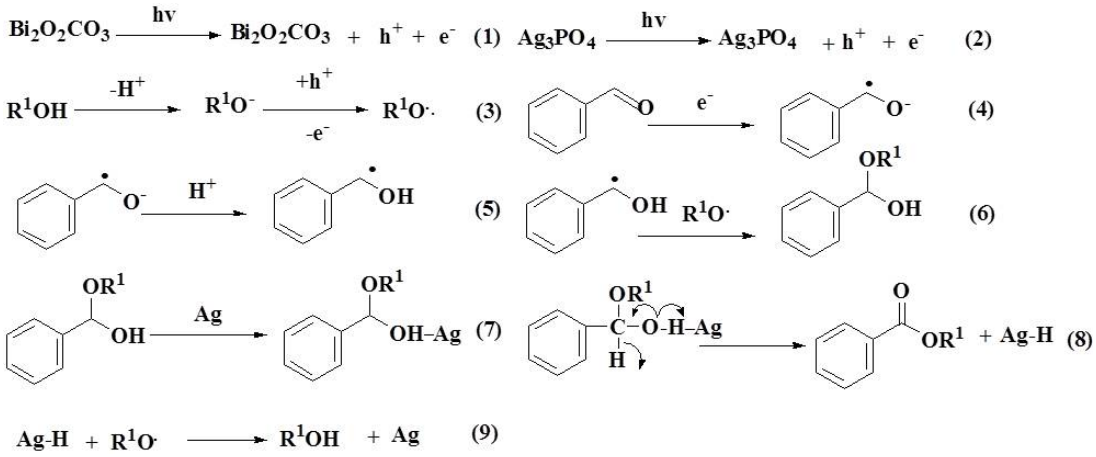

Scheme 1. The reactions of a proposed mechanism for the esterification of aldehydes and alcohols using $Ag_3PO_4/Ag/Bi_2O_2CO_3$.

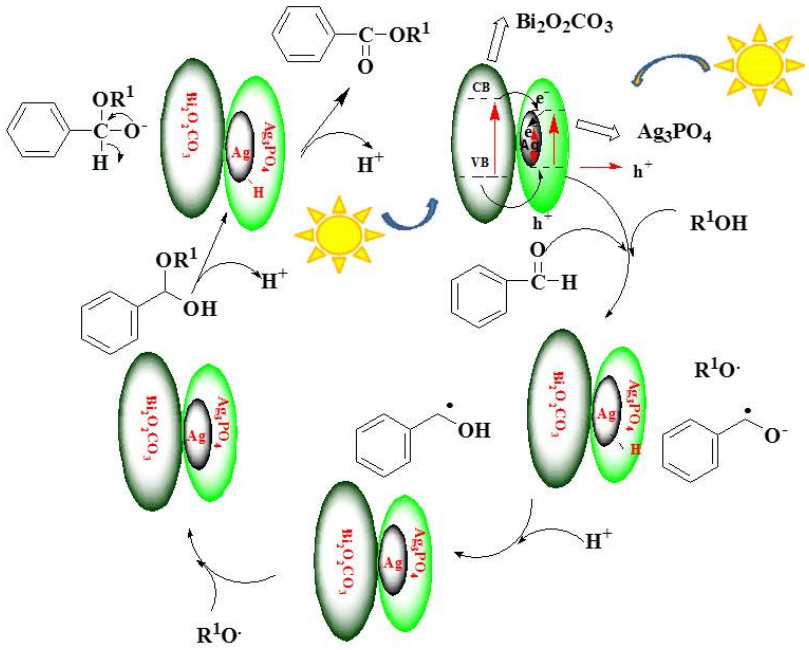

Scheme 2. A proposed mechanism for the esterification of aldehydes and alcohols using $Ag_3PO_4/Ag/Bi_2O_2CO_3$. The yellow sun stands for visible light irradiation.

3. Materials and Methods

3.1. Preparation of Composites

3.1.1. Preparation of $Bi_2O_2CO_3$ Porous Microspheres

All chemicals were used without further purification as they were of analytical grade. The porous $Bi_2O_2CO_3$ microspheres were synthesized with a hydrothermal reaction method. The process was as follows: First, a certain amount of Bi $(NO_3)_3 \cdot 5H_2O$ was dissolved in 40 mL of dilute HNO_3 solution (1 mol·L^{-1}) and stirred for 10 min. Then, 3 mmol of citric acid was added to the solution to ensure complete dissolution. Next, a certain amount of NaOH aqueous solution was added dropwise into the solution, setting the pH value of the solution to 4–5. Later, the solution was transferred into a 100 mL Teflon-lined stainless steel autoclave, and milky-white precipitates were obtained by a hydrothermal reaction at 180 °C for 24 h. Finally, the precipitate was centrifuged and washed with deionized water and ethanol several times before being dried at 75 °C for 8 h [47].

3.1.2. Preparation of the $Ag_3PO_4/Ag/Bi_2O_2CO_3$ Composite

First, 1.14 g of $Bi_2O_2CO_3$ and 1.0 g of polyvinyl pyrrolidone (PVP) were dissolved in 30 mL of deionized water and stirred for 30 min. Then, 20 mL of an $AgNO_3$ solution of a certain concentration was added dropwise to the mixture and stirred for 30 min in order to partially reduce the Ag+ ions to metallic Ag, depositing Ag on the $Bi_2O_2CO_3$ surface. Next, 20 mL of a Na_3PO_4 solution with a certain concentration was added dropwise to the suspension and stirred for a further 5 h to give a 3:1 molar ratio of Ag^+ and PO_4^{3+}. Finally, the mixture was centrifuged, washed with deionized water and ethanol several times, and dried at 60 °C. Consequently, a range of $Ag_3PO_4/Ag/Bi_2O_2CO_3$ products was created with mass percentages of 57 wt %, 64 wt %, 68 wt %, 71 wt %, and 73 wt % Ag_3PO_4 denoted as the 57 wt % $Ag_3PO_4/Ag/Bi_2O_2CO_3$ composite, 64 wt % $Ag_3PO_4/Ag/Bi_2O_2CO_3$ composite, 68 wt % $Ag_3PO_4/Ag/Bi_2O_2CO_3$ composite, 71 wt % $Ag_3PO_4/Ag/Bi_2O_2CO_3$ composite, and 73 wt % $Ag_3PO_4/Ag/Bi_2O_2CO_3$ composite, respectively [22].

3.1.3. Preparation of the $Ag_3PO_4/Bi_2O_2CO_3$ Composite

A similar method was applied to prepare catalysts with the 64 wt % $Ag_3PO_4/Bi_2O_2CO_3$. Typically, 1.14 g of $Bi_2O_2CO_3$ and 1.0 g of polyvinyl pyrrolidone (PVP) were dissolved in 30 mL of deionized water and stirred for 30 min. Then, 20 mL of a Na_3PO_4 solution of a certain concentration was added dropwise to the mixture and stirred for 30 min. Next, 20 mL of an $AgNO_3$ solution of a certain concentration was added dropwise to the suspension and stirred for a further 5 h to achieve a 3:1 molar ratio of Ag^+ and PO_4^{3+}. Finally, the mixture was centrifuged and washed with deionized water and ethanol several times before being dried at 60 °C.

3.1.4. Preparation of the $Ag/Bi_2O_2CO_3$ Composite

The 10 wt % $Ag/Bi_2O_2CO_3$ was prepared as follows: first, 1.14 g of $Bi_2O_2CO_3$ was dissolved in 30 mL of deionized water and stirred for 30 min. Then, 10 mL of an $AgNO_3$ solution of a certain concentration was added dropwise to the mixture and stirred for 4 h. Ag nanoparticles were generated by a 300 W UV lamp for 1 h with constant stirring. Finally, the mixture was centrifuged and washed with deionized water and ethanol several times before being dried at 60 °C [47].

3.2. Characterization

The crystal phases of the samples were analyzed by X-ray diffraction (XRD) (Rigaku Industrial Corporation, Osaka, Japan) with a RIGAKU D/MAX-2500 X-ray diffractometer using Cu Kα radiation (λ = 1.5405 Å) at 40 kV and 100 mA. X-ray photoelectron spectroscopy (XPS) with Al Kα X-ray (hν = 1486.6 eV) radiation operating at 150 W (Escalab 250xi, Thermo Fisher Scientific Company, Waltham, MA, USA) was applied to investigate the surface properties. Scanning electron microscopy (SEM model S-4800, Hitachi Limited Company, Tokyo, Japan) was used to characterize the morphology of the obtained composites. The morphology and structure of the samples were examined by transmission electron microscopy (TEM) (FEI Company, Hillsborough, OR, USA) using an FEI Tecnai G2 F20 S-Twin electron microscope, which was operated at an acceleration voltage of 200 kV. A multipoint BET method was applied to determine the Brunauer-Emmett-Teller (BET) (Quantachrome Instruments, Corporate Headquarters, Boynton Beach, FL, USA) specific surface areas. The UV-vis diffuse reflectance spectra (UV-vis DRS) (Hitachi Limited Company, Tokyo, Japan) of the solid samples were obtained using a scanning UV-vis spectrophotometer (U-3900, Hitachi) equipped with an integrated sphere assembly with 100% $BaSO_4$ as the reflectance sample. The reaction products were quantitatively analyzed with a GC-2014C gas chromatograph (GC-2014C) (Shimadzu Company, Kyoto, Japan). The identity of the product was confirmed with a Trace DSQ II gas chromatograph-mass spectrometer (GC-MS) (Finnigan Company, Silicon valley, CA, USA) at Inner Mongolia University.

3.3. Photo-Catalytic Activity Test

3.3.1. The Esterification Reaction of Aldehydes (or Alcohols) and Alcohols

The catalytic esterification of benzaldehyde (or benzyl alcohol) with other alcohols was detected. In a typical reaction, benzaldehyde (or benzyl alcohol, 1.0 mmol), 8 mL of methanol, and the photo-catalyst (30 mg) were mixed together. No base was added into the aldehyde/alcohol mixtures, but a base was added into the alcohol/alcohol mixtures. The flask was then irradiated with a 500 W Philips halogen lamp (wavelength between 400 and 800 nm) under magnetic stirring and in an Ar (for the esterification of aldehydes and alcohols) or air atmosphere (for the esterification of alcohols and alcohols). The conversion and selectivity of the esterification reactions were calculated from the results detected by GC. The products were qualified using GC-MS [63].

3.3.2. The Amination Reaction of Alcohols and Amines

To detect the amination of benzyl alcohol and aniline, benzyl alcohol (1.0 mmol), aniline (0.5 mmol), 6 mL of solvents, base, and the photo-catalyst (30 mg) were mixed together in an air atmosphere. The other conditions were kept the same as in Section 3.3.1.

3.4. Reuse of the Catalyst

Based on the excellent activities of the 71 wt % $Ag_3PO_4/Ag/Bi_2O_2CO_3$ composite, the following experiment was conducted to demonstrate its ability to be recycled. First, 24 group experiments were performed under identical reaction conditions (benzaldehyde (1.0 mmol), methanol (8 mL), 71 wt % $Ag_3PO_4/Ag/Bi_2O_2CO_3$ catalyst (30 mg), Ar atmosphere, exposure time of 24 h, and light intensity of 4.3×10^{-2} W·cm^{-2}). The catalyst and reactant were centrifuged. The catalyst was then washed with H_3PO_4 (0.1 mol·L^{-1}) and ethanol. Second, using the reused catalysts under the same reaction conditions as above-mentioned, 18 group experiments were conducted simultaneously. Third, the thrice-used catalyst was employed for a further 12 group experiments under the same reaction conditions. Fourth, eight group experiments were conducted using the fourth-used catalyst under the same reaction conditions, followed by an additional six group experiments conducted using the catalyst already used four times under the same reaction conditions. Finally, three group experiments were analyzed with the catalyst already used five times under the same conditions. The results are shown in Figure S2.

4. Conclusions

$Ag_3PO_4/Ag/Bi_2O_2CO_3$ composites were fabricated by a joint hydrothermal and precipitation method. The heterogeneous catalyst (71 wt % $Ag_3PO_4/Ag/Bi_2O_2CO_3$) displayed good reactivity in the esterification of aldehydes (or alcohols) and alcohols, and in the synthesis of imines through alcohols and amines under visible light irradiation. The catalyst was stable and could be used at least six times. Visible light was applied for the reaction process at low temperature. These conditions were more advantageous than other systems reported to date. A possible reaction pathway from aldehydes and alcohols to esters was described.

Supplementary Materials: The following are available online at www.mdpi.com/2073-4344/7/9/276/s1, Figure S1: SEM images of the photo-catalysts (a,b) $Bi_2O_2CO_3$ (c,d) 10 wt % $Ag/Bi_2O_2CO_3$ (e,f) 64 wt % $Ag_3PO_4/Bi_2O_2CO_3$ (g,h) 71 wt % $Ag_3PO_4/Ag/Bi_2O_2CO_3$ (i,j) reused 71 wt % $Ag_3PO_4/Ag/Bi_2O_2CO_3$, Figure S2: Photo-catalytic activity of the 71 wt % $Ag_3PO_4/Ag/Bi_2O_2CO_3$ catalyst after being used for 6 times, Figure S3: EDX image of 71 wt % $Ag_3PO_4/Ag/Bi_2O_2CO_3$ after reusing, Table S1: BET surface areas of the photo-catalysts supported on $Bi_2O_2CO_3$ and $Bi_2O_2CO_3$, Table S2: Synthesis of esters from benzyl alcohol and methanol using 71 wt % $Ag_3PO_4/Ag/Bi_2O_2CO_3$, Table S3: Synthesis of imines from benzyl alcohol and aniline using 71wt % $Ag_3PO_4/Ag/Bi_2O_2CO_3$.

Acknowledgments: This work was financially supported by the National Natural Science Foundation of China (NSFC, No. 20567002, No. 21067007 and No. 21167008), the Natural Science Fund of Inner Mongolia (2010MS0203 and 2014MS0201), the 2013 Annual Grassland Talents Project of Inner Mongolia Autonomous Region, and the 2013 Annual Inner Mongolia Talent Development Fund.

Author Contributions: Zhi Guo and Jingyi Li conceived and designed the experiments; Zhi Guo performed the experiments, analyzed the data, and wrote the manuscript. Hui Xin, Jingjing Ma, Meifen Bai, and Yan Wang participated in the design of the study and assisted in drafting the manuscript. All authors read and approved the final manuscript.

Conflicts of Interest: The authors declare no conflict of interest.

References

1. Jagadeesh, R.V.; Junge, H.; Pohl, M.M.; Radnik, J.; Bruckner, A.; Beller, M. Selective oxidation of alcohols to ester using heterogeneous Co_3O_4-N@C catalysts under mild conditions. *J. Am. Chem. Soc.* **2013**, *135*, 10776–10782. [CrossRef] [PubMed]
2. Larock, R.C. *Comprehensive Organic Transformations: A Guide to Functional Group Preparations*; Wiley-VCH Press: New York, NY, USA, 1989.
3. Sarkar, S.D.; Grimme, S.; Studer, A. NHC catalyzed oxidations of aldehydes to esters: Chemoselective acylation of alcohols in presence of amines. *J. Am. Chem. Soc.* **2010**, *132*, 1190–1191. [CrossRef] [PubMed]
4. Li, Q.Q.; Xiao, Z.F.; Yao, C.Z.; Zheng, H.X.; Kang, Y.B. Direct alkylation of amines with alcohols catalyzed by base. *Org. Lett.* **2015**, *17*, 5328–5331. [CrossRef] [PubMed]
5. Reddy, R.S.; Rosa, J.N.; Veiros, L.F.; Caddick, S.; Gois, P.M.P. NHC/iron cooperative catalysis: Aerobic oxidative esterification of aldehydes with phenols. *Org. Biomol. Chem.* **2011**, *9*, 3126–3129. [CrossRef] [PubMed]
6. Kawahara, R.; Fujita, K.I.; Yamaguchi, R. N-alkylation of amines with alcohols catalyzed by a water soluble Cp*iridium complex: An efficient method for the synthesis of amines in aqueous media. *Adv. Synth. Catal.* **2011**, *353*, 1161–1168. [CrossRef]
7. Kiyooka, S.I.; Wada, Y.; Ueno, M.; Yokoyama, T.; Yokoyama, R. $[IrCl(cod)]_2$-catalyzed direct oxidative esterification of aldehydes with alcohols. *Tetrahedron* **2007**, *63*, 12695–12701. [CrossRef]
8. Bolm, C.; Legros, J.; Paih, J.L.; Zani, L. Iron-catalyzed reactions in organic synthesis. *Chem. Rev.* **2004**, *104*, 6217–6254. [CrossRef] [PubMed]
9. Rout, S.K.; Guin, S.; Ghara, K.K.; Banerjee, A.; Patel, B.K. Copper catalyzed oxidative esterification of aldehydes with alkylbenzenes via cross dehydrogenative coupling. *Org. Lett.* **2012**, *14*, 3982–3985. [CrossRef] [PubMed]
10. Yoo, W.J.; Li, C.J. Copper-catalyzed oxidative esterification of alcohols with aldehydes activated by lewis acids. *Tetrahedron Lett.* **2007**, *48*, 1033–1035. [CrossRef]
11. Liu, C.; Tang, S.; Zheng, L.W.; Liu, D.; Zhang, H.; Lei, A.W. Covalently bound benzyl ligand promotes selective palladium catalyzed oxidative esterification of aldehydes with alcohols. *Angew. Chem. Int. Ed.* **2012**, *51*, 5662–5666. [CrossRef] [PubMed]
12. Liu, P.; Li, C.; Hensen, E.J.M. Efficient tandem synthesis of methyl esters and imines by using versatile hydrotalcite-supported gold nanoparticles. *Chem. Eur. J.* **2012**, *18*, 12122–12129. [CrossRef] [PubMed]
13. Abiko, A.; Roberts, J.C.; Takemasa, T.; Masamune, S. $KMnO_4$ revisited: Oxidation of aldehydes to carboxylic acids in the tert-butyl alcohol-aqueous NaH_2PO_4 system. *Tetrahedron Lett.* **1986**, *27*, 4537–4540. [CrossRef]
14. Garegg, P.J.; Olsson, L.; Oscarson, S. Synthesis of methyl (ethyl 2-*O*-acyl-3,4-di-*O*-benzyl-1-thio-β-D-glucopyr anosid) uronates and evaluation of their use as reactive β-selective glucuronic acid donors. *J. Org. Chem.* **1995**, *60*, 2200–2204. [CrossRef]
15. Qian, G.; Zhao, R.; Ji, D.; Lu, G.M.; Qi, Y.X.; Suo, J.S. Facile oxidation of aldehydes to esters using S-SnO_2/SBA-1-H_2O_2. *Chem. Lett.* **2004**, *33*, 834–835. [CrossRef]
16. Travis, B.R.; Sivakumar, M.; Hollist, G.O.; Borhan, B. Facile oxidation of aldehydes to acids and esters with oxone. *Org. Lett.* **2003**, *5*, 1031–1034. [CrossRef] [PubMed]
17. McDonald, C.; Holcomb, H.; Kennedy, K.; Kirkpatrick, E.; Leathers, T.; Vanemon, P. *N*-iodosuccinimide-mediated conversion of aldehydes to methyl esters. *J. Org. Chem.* **1989**, *54*, 1213–1215. [CrossRef]
18. Gopinah, R.; Barkakaty, B.; Talukdar, B.; Patel, B.K. Peroxovanadium-catalyzed oxidative esterification of aldehydes. *J. Org. Chem.* **2003**, *68*, 2944–2947. [CrossRef] [PubMed]
19. Enthaler, S.; Junge, K.; Beller, M. Sustainable metal catalysis with iron: From rust to a rising star. *Angew. Chem. Int. Ed.* **2008**, *47*, 3317–3321. [CrossRef] [PubMed]
20. Hao, Y.J.; Chong, Y.Z.; Li, S.R.; Yang, H.Q. Controlled synthesis of Au nanoparticles in the nanocages of SBA-16: Improved activity and enhanced recyclability for the oxidative esterification of alcohols. *J. Phys. Chem. C* **2012**, *116*, 6512–6519. [CrossRef]
21. Zhang, Y.L.; Xiao, Q.; Bao, Y.S.; Zhang, Y.J.; Bottle, S.; Sarina, S.; Bao, Z.R.G.T.; Zhu, H.Y. Direct photocatalytic conversion of aldehydes to esters using supported gold nanoparticles under visible light irradiation at room temperature. *J. Phys. Chem. C* **2014**, *118*, 19062–19069. [CrossRef]

22. Bu, Y.Y.; Chen, Z.Y.; Sun, C.J. Highly efficient Z-scheme $Ag_3PO_4/Ag/WO_{3-x}$ photocatalyst for its enhanced photocatalytic performance. *Appl. Catal. B* **2015**, *179*, 363–371. [CrossRef]
23. Zhang, L.W.; Man, Y.; Zhu, Y.F. Effects of Mo replacement on the structure and visible-light-induced photocatalytic performances of Bi_2WO_6 photocatalyst. *ACS Catal.* **2011**, *1*, 841–848. [CrossRef]
24. Ruan, Q.J.; Zhang, W.D. Tunable morphology of $Bi_2Fe_4O_9$ crystals for photocatalytic oxidation. *J. Phys. Chem. C* **2009**, *113*, 4168–4173. [CrossRef]
25. Xiao, X.; Zhang, W.D. Facile synthesis of nanostructured BiOI microspheres with high visible light-induced photocatalytic activity. *J. Mater. Chem.* **2010**, *20*, 5866–5870. [CrossRef]
26. Dong, F.; Ho, W.K.; Lee, S.C.; Wu, Z.B.; Fu, M.; Zou, S.C.; Huang, Y. Template-free fabrication and growth mechanism of uniform $(BiO)_2CO_3$ hierarchical hollow microspheres with outstanding photocatalytic activities under both UV and visible light irradiation. *J. Mater. Chem.* **2011**, *21*, 12428–12436. [CrossRef]
27. Liu, Y.Y.; Wang, Z.Y.; Huang, B.B.; Yang, K.S.; Zhang, X.Y.; Qin, X.Y.; Dai, Y. Preparation, electronic structure, and photocatalytic properties of $Bi_2O_2CO_3$ nanosheet. *Appl. Surf. Sci.* **2010**, *257*, 172–175. [CrossRef]
28. Chen, R.; So, M.H.; Yang, J.; Deng, F.; Che, C.M.; Sun, H.Z. Fabrication of bismuth subcarbonate nanotube arrays from bismuth citrate. *Chem. Commun.* **2006**, *21*, 2265–2267. [CrossRef] [PubMed]
29. Chen, R.; Cheng, G.; So, M.H.; Wu, J.L.; Lu, Z.; Che, C.M.; Sun, H.Z. Bismuth subcarbonate nanoparticles fabricated by water-in-oil microemulsion-assisted hydrothermal process exhibit anti-helicobacter pylori properties. *Mater. Res. Bull.* **2010**, *45*, 654–658. [CrossRef]
30. Cheng, H.F.; Huang, B.B.; Yang, K.S.; Wang, Z.Y.; Qin, X.Y.; Zhang, X.Y.; Dai, Y. Facile template-free synthesis of $Bi_2O_2CO_3$ hierarchical microflowers and their associated photocatalytic activity. *Chem. Phys. Chem.* **2010**, *11*, 2167–2173. [CrossRef] [PubMed]
31. Cao, X.F.; Zhang, L.; Chen, X.T.; Xue, Z.L. Persimmon-like $(BiO)_2CO_3$ microstructures: Hydrothermal preparation, photocatalytic properties and their conversion into Bi_2S_3. *Cryst. Eng. Commun.* **2011**, *13*, 1939–1945. [CrossRef]
32. Dong, F.; Lee, S.C.; Wu, Z.B.; Huang, Y.; Fu, M.; Ho, W.K.; Zou, S.C.; Wang, B. Rose-like monodisperse bismuth subcarbonate hierarchical hollow microspheres: One-pot template-free fabrication and excellent visible light photocatalytic activity and photochemical stability for NO removal in indoor air. *J. Hazard. Mater.* **2011**, *195*, 346–354. [CrossRef] [PubMed]
33. Zhao, T.Y.; Zai, J.T.; Xu, M.; Zou, Q.; Su, Y.Z.; Wang, K.X.; Qian, X.F. Hierarchical $Bi_2O_2CO_3$ microspheres with improved visible-light-driven photocatalytic activity. *Cryst. Eng. Commun.* **2011**, *13*, 4010–4017. [CrossRef]
34. Madhusudan, P.; Ran, J.R.; Zhang, J.; Yu, J.G.; Liu, G. Novel urea assisted hydrothermal synthesis of hierarchical $BiVO_4/Bi_2O_2CO_3$ nano composites with enhanced visible-light photocatalytic activity. *Appl. Catal. B* **2011**, *110*, 286–295. [CrossRef]
35. Madhusudan, P.; Yu, J.G.; Wang, W.G.; Cheng, B.; Liu, G. Facile synthesis of novel hierarchical graphene-$Bi_2O_2CO_3$ composites with enhanced photocatalytic performance under visible light. *Dalton Trans.* **2012**, *41*, 14345–14353. [CrossRef] [PubMed]
36. Zhu, G.Q.; Hojamberdievb, M.; Katsumata, K.I.; Cai, X.; Matsushita, N.; Okada, K.; Liu, P.; Zhou, J.P. Heterostructured $Fe_3O_4/Bi_2O_2CO_3$ photocatalyst: Synthesis, characterization and application in recyclable photodegradation of organic dyes under visible light irradiation. *Mater. Chem. Phys.* **2013**, *142*, 95–105. [CrossRef]
37. Zhang, X.C.; Guo, T.Y.; Wang, X.W.; Wang, Y.W.; Fan, C.M.; Zhang, H. Facile composition-controlled preparation and photocatalytic application of $BiOCl/Bi_2O_2CO_3$ nanosheets. *Appl. Catal. B* **2014**, *150*, 486–495. [CrossRef]
38. Bi, Y.P.; Ouyang, S.X.; Umezawa, N.; Cao, J.Y.; Ye, J.H. Facet effect of single-crystalline Ag_3PO_4 sub-microcrystals on photocatalytic properties. *J. Am. Chem. Soc.* **2011**, *133*, 6490–6492. [CrossRef] [PubMed]
39. Hou, Y.; Li, X.Y.; Zhao, Q.D.; Chen, G.H.; Raston, C.L. Role of hydroxyl radicals and mechanism of escherichia coli inactivation on $Ag/AgBr/TiO_2$ nanotube array electrode under visible light irradiation. *Environ. Sci. Technol.* **2012**, *46*, 4042–4050. [CrossRef] [PubMed]
40. Hu, X.X.; Hu, C.; Peng, T.W.; Zhou, X.F.; Qu, J.H. Plasmon-induced inactivation of enteric pathogenic microorganisms with Ag-AgI/Al_2O_3 under visible-light irradiation. *Environ. Sci. Technol.* **2010**, *44*, 7058–7062. [CrossRef] [PubMed]

41. Ghosh, S.; Saraswathi, A.; Indi, S.S.; Hoti, S.L.; Vasan, H.N. Ag@AgI, core@shell structure in agarose matrix as hybrid: Synthesis, characterization, and antimicrobial activity. *Langmuir* **2012**, *28*, 8550–8561. [CrossRef] [PubMed]
42. Tong, H.; Ouyang, S.X.; Bi, Y.P.; Umezawa, N.; Oshikiri, M.; Ye, J.H. Nano-photocatalytic materials: Possibilities and challenges. *Adv. Mater.* **2012**, *24*, 229–251. [CrossRef] [PubMed]
43. Ouyang, S.X.; Ye, J.H. β-$AgAl_{1-x}Ga_xO_2$ solid-solution photocatalysts: Continuous modulation of electronic structure toward high-performance visible-light photoactivity. *J. Am. Chem. Soc.* **2011**, *133*, 7757–7763. [CrossRef] [PubMed]
44. Umezawa, N.; Ouyang, S.X.; Ye, J.H. Theoretical study of high photocatalytic performance of Ag_3PO_4. *Phys. Rev. B* **2011**, *83*, 035202(1–8). [CrossRef]
45. Boltersdorf, J.; Wong, T.; Maggard, P.A. Synthesis and optical properties of Ag(I), Pb(II), and Bi(III) tantalate-based photocatalysts. *ACS Catal.* **2013**, *3*, 2943–2953. [CrossRef]
46. Yi, Z.G.; Ye, J.H.; Kikugawa, N.; Kako, T.; Ouyang, S.X.; Williams, H.S.; Yang, H.; Cao, J.Y.; Luo, W.J.; Li, Z.S.; et al. An orthophosphate semiconductor with photooxidation properties under visible-light irradiation. *Nat. Mater.* **2010**, *9*, 559–564. [CrossRef] [PubMed]
47. Lei, J.; Zhu, G.Q.; Hojamberdiev, M.; Luo, X.C.; Tan, C.W.; Peng, J.H.; Wei, X.M.; Li, J.P.; Liu, P. A plasmonic Ag-AgBr/$Bi_2O_2CO_3$ composite photocatalyst with enhanced visible-light photocatalytic activity. *Ind. Eng. Chem. Res.* **2014**, *53*, 13718–13727.
48. Chen, X.; Zheng, Z.F.; Ke, X.B.; Jaatinen, E.; Xie, T.F.; Wang, D.J.; Guo, C.; Zhao, J.C.; Zhu, H.Y. Supported silver nanoparticles as photocatalysts under ultraviolet and visible light irradiation. *Green Chem.* **2010**, *12*, 414–419. [CrossRef]
49. Yu, C.L.; Zhou, W.Q.; Zhu, L.H.; Li, G.; Yang, K.; Jin, R.C. Integrating plasmonic Au nanorods with dendritic like α-Bi_2O_3/$Bi_2O_2CO_3$ heterostructures for superior visible-light-driven photocatalysis. *Appl. Catal. B* **2016**, *184*, 1–11. [CrossRef]
50. Chen, Z.H.; Wang, W.L.; Zhang, Z.G.; Fang, X.M. High-efficiency visible-light-driven Ag_3PO_4/AgI photocatalysts: Z-scheme photocatalytic mechanism for their enhanced photocatalytic activity. *J. Phys. Chem. C* **2013**, *117*, 19346–19352. [CrossRef]
51. Zhu, M.S.; Chen, P.L.; Liu, M.H. Visible-light-driven Ag/Ag_3PO_4-based plasmonic photocatalysts: Enhanced photocatalytic performance by hybridization with graphene oxide. *Chin. Sci. Bull.* **2013**, *58*, 84–91. [CrossRef]
52. Dong, F.; Sun, Y.J.; Fu, M.; Ho, W.K.; Lee, S.C.; Wu, Z.B. Novel in situ N-doped $(BiO)_2CO_3$ hierarchical microspheres self-assembled by nanosheets as efficient and durable visible light driven photocatalyst. *Langmuir* **2012**, *28*, 766–773. [CrossRef] [PubMed]
53. Katsumata, H.; Sakai, T.; Suzuki, T.; Kaneco, S. Highly efficient photocatalytic activity of g-C_3N_4/Ag_3PO_4 hybrid photocatalysts through Z-scheme photocatalytic mechanism under visible light. *Ind. Eng. Chem. Res.* **2014**, *53*, 8018–8025. [CrossRef]
54. Li, W.J.; Li, D.Z.; Chen, Z.X.; Huang, H.J.; Sun, M.; He, Y.H.; Fu, X.Z. High-efficient degradation of dyes by $Zn_xCd_{1-x}S$ solid solutions under visible light irradiation. *J. Phys. Chem. C* **2008**, *112*, 14943–14947. [CrossRef]
55. Sarina, S.; Zhu, H.Y.; Xiao, Q.; Jaatinen, E.; Jia, J.F.; Huang, Y.M.; Zheng, Z.F.; Wu, H.S. Viable photocatalysts under solar-spectrum irradiation: Nonplasm onic metal nanoparticles. *Angew. Chem. Int. Ed.* **2014**, *53*, 2935–2940. [CrossRef] [PubMed]
56. Yu, J.; Li, J.Y.; Wei, H.L.; Zheng, J.W.; Su, H.Q.; Wang, X.J. Hydrotalcite-supported gold catalysts for a selective aerobic oxidation of benzyl alcohol driven by visible light. *J. Mol. Catal. A* **2014**, *395*, 128–136. [CrossRef]
57. Wei, H.L.; Li, J.Y.; Yu, J.; Zheng, J.W.; Su, H.Q.; Wang, X.J. Gold nanoparticles supported on metal oxides as catalysts for the direct oxidative esterification of alcohols under mild conditions. *Inorg. Chim. Acta* **2015**, *427*, 33–40. [CrossRef]
58. Shimura, K.; Shimizu, K.I. Transfer hydrogenation of ketones by ceria-supported Ni catalysts. *Green Chem.* **2012**, *14*, 2983–2985. [CrossRef]
59. Cano, R.; Yus, M.; Ramón, D.J. First practical cross-alkylation of primary alcohols with a new and recyclable impregnated iridium on magnetite catalyst. *Chem. Commun.* **2012**, *48*, 7628–7630. [CrossRef] [PubMed]
60. Suzuki, K.; Yamaguchi, T.; Matsushita, K.; Iitsuka, C.; Miura, J.; Akaogi, T.; Ishida, H. Aerobic oxidative esterification of aldehydes with alcohols by gold-nickel oxide nanoparticle catalysts with a core-shell structure. *ACS Catal.* **2013**, *3*, 1845–1849. [CrossRef]

61. Bowling, N.P.; Mcmahon, R.J. Enediyne isomers of tetraethynylethene. *J. Org. Chem.* **2006**, *71*, 5841–5847. [CrossRef] [PubMed]
62. Kim, Y.J.; Kim, N.Y.; Cheon, C.H. Beyond benzoin condensation: Trimerization of aldehydes via metal-free aerobic oxidative esterification of aldehydes with benzoin products in the presence of cyanide. *Org. Lett.* **2014**, *16*, 2514–2517. [CrossRef] [PubMed]
63. Zheng, J.W.; Li, J.Y.; Wei, H.L.; Yu, J.; Su, H.Q.; Wang, X.J. The investigation of gold/zirconia as a photocatalyst for the direct synthesis of imine from alcohols and aniline. *Mater. Sci. Semicond. Process.* **2015**, *32*, 131–136. [CrossRef]